Energy 36 (2011) 5065–5080

Contents lists available at ScienceDirect

Energy

journal homepage: www.elsevier.com/locate/energy

Entropy generation due to natural convection in discretely heated porous square cavities

Ram Satish Kaluri, Tanmay Basak*

Department of Chemical Engineering, Indian Institute of Technology Madras, Chennai-600036, India

ARTICLE INFO

Article history:
Received 8 September 2010
Received in revised form
30 May 2011
Accepted 1 June 2011
Available online 19 July 2011

Keywords:
Entropy
Natural convection
Discrete heating
Square cavity

ABSTRACT

Optimization of industrial processes for higher energy efficiency may be effectively carried out based on the thermodynamic approach of entropy generation minimization (EGM). This approach provides the key insights on how the available energy (exergy) is being destroyed during the process and the ways to minimize its destruction. In this study, EGM approach is implemented for the analysis of optimal thermal mixing and temperature uniformity due to natural convection in square cavities filled with porous medium for the material processing applications. Effect of the permeability of the porous medium and the role of distributed heating in enhancing the thermal mixing, temperature uniformity and minimization of entropy generation is analyzed. It is found that at lower Darcy number (*Da*), the thermal mixing is low and the heat transfer irreversibility dominates the total entropy generation. In contrast, thermal mixing is improved due to enhanced convection at higher *Da*. Friction irreversibility is found to dominate the total entropy generation for higher Prandtl number (*Pr*) fluids at higher *Da*, whereas the heat transfer irreversibility dominates the total entropy generation for lower *Pr* fluids. Based on EGM analysis, it is established that larger thermal mixing at high Darcy number may not be always recommended as the total entropy production is quite large at high Darcy number. Overall, it is found that the distributed heating methodology with multiple heat sources may be an efficient strategy for the optimal thermal processing of materials.

1. Introduction

EGM (entropy generation minimization) is a thermodynamic approach of optimization of engineering systems for higher energy efficiency [1,2]. The EGM approach has been applied to optimize various systems such as microchannels [3], fuel cells [4], heat exchangers [5,6], environmental control of aircraft [7], combustion in porous media [8], reactors [9], power generation [10], thermal storage [11], diesel engines [12], two-phase flow [13] and solar-related applications [14,15].

Natural convection in porous enclosures with discrete heat sources has important applications in electronic packaging [16], cooling of nuclear reactors [17], ignition of solid fuels [18] etc. El-Khatib and Prasad [19] numerically investigated the effects of stratification on thermal convection in a horizontal cavity filled with fluid-saturated porous medium with a localized heat source on the bottom surface and varying the temperature linearly on the side walls. Robillard et al. [20] studied the multiple steady states in a confined porous medium with localized heating from the below. Lai and Kulacki [21] performed numerical and experimental studies on free and mixed convection in horizontal porous layers with multiple, isothermal, discrete heat source for various Rayleigh and Peclet numbers. Hsiao et al. [22] solved the problem of natural convection in an inclined porous cavity with discrete heat source on a wall. Effects of variable heat source spacing and heat source width on the enhancement of heat transfer and pressure drop in a partially porous channel with discrete heat sources were analyzed by Hadim and Bethancourt [23]. Heindel et al. [24] performed experimental and numerical studies on natural convection heat transfer by modelling dense parallel plate fin array on discrete heat sources as a porous medium. Saeid and Pop [25] numerically studied the natural convection in porous square cavity with a discrete heat source on a vertical wall with isothermal and isoflux boundary conditions. Recently, double-diffusive convective flow of a binary mixture in a porous enclosure subject to localized heating and salting from one side was studied by Zhao et al. [26].

Application of EGM method for the optimization of natural convection in porous square cavities with discrete heat sources may be helpful in enhancing the thermodynamic efficiency of the

* Corresponding author. Tel.: +91 44 2257 4173; fax: +91 44 2257 0509.
E-mail addresses: ramsatish@che.iitm.ac.in (R.S. Kaluri), tanmay@iitm.ac.in (T. Basak).

0360-5442/$ – see front matter © 2011 Elsevier Ltd. All rights reserved.
doi:10.1016/j.energy.2011.06.001

system. Further, with the knowledge of irreversibilities present in the system, the porous medium (such as metal foams for electronic cooling applications) can be *designed* with desirable characteristics. In a thermal convection system, the irreversibilities are due to heat transfer and fluid friction. Perusal of literature reveals that, only few studies have been reported on the entropy generation due to natural convection in enclosures filled with porous media. Baytas [27] studied the entropy generation in a differentially heated inclined square porous cavity and analyzed the effect of Darcy modified Rayleigh number and Bejan number on the entropy generation for various degrees of inclination. Mahmud et al. [28] have studied the entropy generation characteristics in wavy enclosures filled with microstructures that were modeled as porous medium. They reported that the high irreversibility is exhibited in cavities with lower aspect ratio in the phase-plus mode, while higher aspect ratio in the phase-minus mode exhibit low irreversibility. Zahmatkesh [29] investigated the effect of thermal boundary conditions on the entropy generation in a porous cavity with a hot bottom wall and cold side walls and found that the entropy generation rate is high for uniform heating of the isothermal bottom wall case compared to the non-uniform heating case. Further, Varol et al. [30] have numerically studied the entropy generation due to natural convection in non-uniformly heated porous isosceles triangular enclosure positioned at various inclinations and they concluded that the highest entropy generation due to heat transfer and fluid friction is observed at $\Phi = 90^{\circ}$. To authors' knowledge, the studies on entropy generation due to natural convection in porous enclosures with discrete heat sources have not been reported till date and that forms the objective of the current study.

The aim of this study is to analyze the entropy generation during natural convection in porous square cavities that are heated differentially and discretely. A square cavity involving the isothermal hot bottom wall, the cold side walls and an adiabatic top wall is considered initially. The entropy generation for the case with isothermal hot bottom wall is studied and that is compared with entropy generation for two other configurations where the square cavities are heated with discrete isothermal heat sources as shown in Fig. 1. This analysis has significance in thermal processing applications such as molten metals infiltration in porous media [31], drying and transport of gases in porous media [32], enhanced oil recovery by hot-water flooding in porous beds [33], combustion of heavy oils in porous reservoirs [34] etc. A generalized non-Darcy model proposed by Vafai and Tien [35], with Forchheimer inertia term being neglected, is employed to model the porous medium. In the current study, Galerkin finite element method has been employed to solve the non-linear equations of fluid flow, energy and entropy. Simulations are carried out for a range of parameters, $Da = 10^{-3}$–10^{-6}, $Ra = 10^{3}$–10^{6} and $Pr = 0.015$ (molten metals), 0.7 (air or gaseous substances), 10 (aqueous solutions), 1000 (olive/engine oils). A detailed analysis on the effect of permeability of porous medium on the entropy generation due to heat transfer and fluid friction irreversibilities is presented via local entropy maps. Further, the influence of Darcy number on the variation of total entropy generation and on the competition of thermal and frictional irreversibilities in various cases is presented.

2. Mathematical formulation and simulation

The physical domains of different cases are shown in Fig. 1(a)–(c). Isothermal heat sources are represented by thick lines and the remaining sections are maintained cold isothermal except for the top adiabatic wall. The total dimensionless length of the heat sources in cases 2 and 3 is equal to 1, which is same as that in

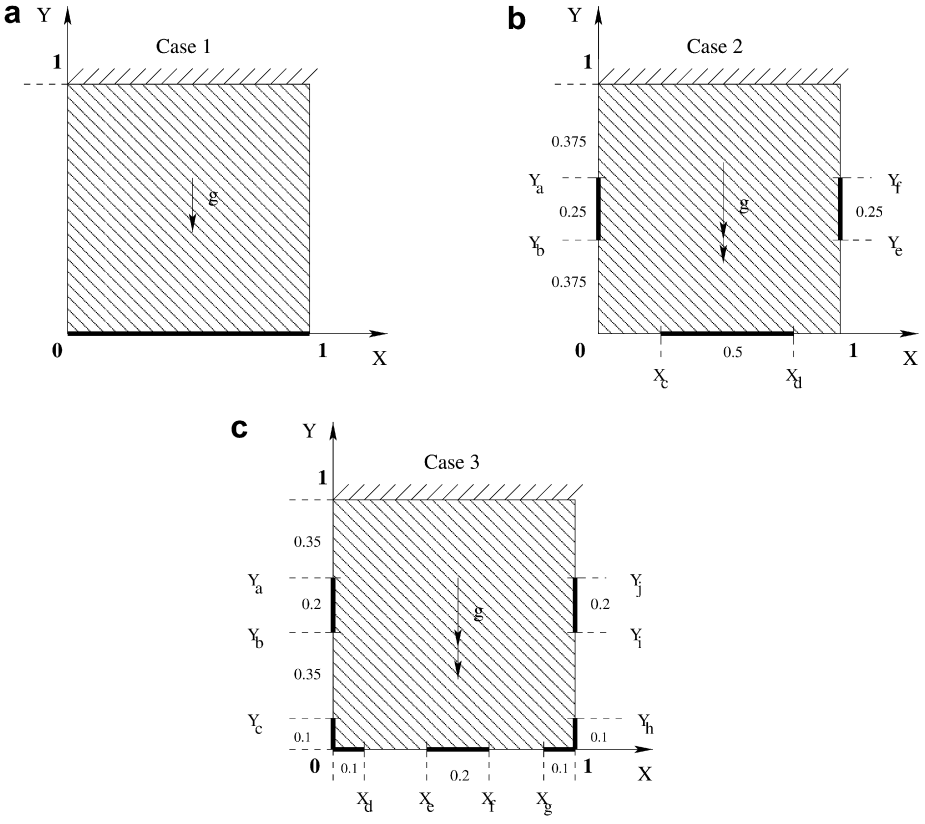

Fig. 1. Schematic diagrams of the cavities for different cases. Top wall is adiabatic. Thick line represents the uniformly heated section while remaining sections are maintained cold.

case 1. All the physical properties are assumed to be constant, except the density in buoyancy term. The change in density due to temperature variation is calculated using Boussinesq approximation. Another important assumption is that the local thermal equilibrium (LTE) is valid i.e., the temperature of the fluid phase is equal to the temperature of the solid phase everywhere in the porous region. The momentum transfer in porous medium is based on generalized non-Darcy model proposed by Vafai and Tien [35]. However, the velocity square term or Forchheimer term which models the inertia effect is neglected here as in the present case, only natural convection flow in porous medium is studied in an enclosed cavity. The inertia effect is more important for large fluid velocities in a high-porosity medium. Similar approximation of negligible inertial effects was considered by earlier researchers [36–38]. Under these assumptions and following Vafai and Tien [35] with Forchheimer inertia term being neglected, the governing equations for the steady two-dimensional natural convection flow in a porous square cavity using conservation of mass, momentum and energy may be written with following dimensionless variables or numbers:

$$X=\frac{x}{L},\quad Y=\frac{y}{L},\quad U=\frac{uL}{\alpha},\quad V=\frac{vL}{\alpha},\quad \theta=\frac{T-T_c}{T_h-T_c}$$
$$P=\frac{pL^2}{\rho\alpha^2},\quad \mathrm{Pr}=\frac{\nu}{\alpha},\quad Da=\frac{K}{L^2},\quad Ra=\frac{g\beta(T_h-T_c)L^3\mathrm{Pr}}{\nu^2} \tag{1}$$

as:

$$\frac{\partial U}{\partial X}+\frac{\partial V}{\partial Y}=0 \tag{2}$$

$$U\frac{\partial U}{\partial X}+V\frac{\partial U}{\partial Y}=-\frac{\partial P}{\partial X}+\mathrm{Pr}\left(\frac{\partial^2 U}{\partial X^2}+\frac{\partial^2 U}{\partial Y^2}\right)-\frac{\mathrm{Pr}}{Da}U \tag{3}$$

$$U\frac{\partial V}{\partial X}+V\frac{\partial V}{\partial Y}=-\frac{\partial P}{\partial Y}+\mathrm{Pr}\left(\frac{\partial^2 V}{\partial X^2}+\frac{\partial^2 V}{\partial Y^2}\right)-\frac{\mathrm{Pr}}{Da}V+Ra\,\mathrm{Pr}\,\theta \tag{4}$$

$$U\frac{\partial \theta}{\partial X}+V\frac{\partial \theta}{\partial Y}=\frac{\partial^2 \theta}{\partial X^2}+\frac{\partial^2 \theta}{\partial Y^2} \tag{5}$$

The boundary conditions for velocities are

$$U(X,0)=U(X,1)=U(0,Y)=U(1,Y)=0$$
$$V(X,0)=V(X,1)=V(0,Y)=V(1,Y)=0 \tag{6}$$

and the boundary conditions for temperature with cases 1–4 are

$$\theta=1\ (\text{for hot regime})$$
$$\theta=0\ (\text{for cold regime})$$
$$\frac{\partial\theta}{\partial Y}=0\ (\text{for adiabatic wall}) \tag{7}$$

Note that, in Eqs. (1)–(7), X and Y are dimensionless coordinates varying along horizontal and vertical directions, respectively; U and V are dimensionless velocity components in the X and Y directions, respectively; θ is the dimensionless temperature; P is the dimensionless pressure; Ra, Pr and Da are Rayleigh, Prandtl and Darcy numbers, respectively.

The momentum and energy balance equations [Eqs. (3)–(5)] are solved using the Galerkin finite element method. The continuity equation (Eq. (2)) has been used as a constraint due to mass conservation and this constraint may be used to obtain the pressure distribution. In order to solve Eqs. (3) and (4), we use the penalty finite element method where the pressure, P is eliminated by a penalty parameter, γ and the incompressibility criteria given by Eq. (2) which results in

$$P=-\gamma\left(\frac{\partial U}{\partial X}+\frac{\partial V}{\partial Y}\right) \tag{8}$$

The continuity equation [Eq. (2)] is automatically satisfied for large values of γ. Typical value of γ that yields consistent solutions is 10^7. Using Eq. (8), the momentum balance equations [Eqs. (3) and (4)] reduce to

$$U\frac{\partial U}{\partial X}+V\frac{\partial U}{\partial Y}=\gamma\frac{\partial}{\partial X}\left(\frac{\partial U}{\partial X}+\frac{\partial V}{\partial Y}\right)+\mathrm{Pr}\left(\frac{\partial^2 U}{\partial X^2}+\frac{\partial^2 U}{\partial Y^2}\right)-\frac{\mathrm{Pr}}{Da}U \tag{9}$$

and

$$U\frac{\partial V}{\partial X}+V\frac{\partial V}{\partial Y}=\gamma\frac{\partial}{\partial Y}\left(\frac{\partial U}{\partial X}+\frac{\partial V}{\partial Y}\right)+\mathrm{Pr}\left(\frac{\partial^2 V}{\partial X^2}+\frac{\partial^2 V}{\partial Y^2}\right)-\frac{\mathrm{Pr}}{Da}V+Ra\,\mathrm{Pr}\,\theta \tag{10}$$

Expanding the velocity components (U, V) and temperature (θ) using the basis set $\{\Phi_k\}_{k=1}^N$ as,

$$U\approx\sum_{k=1}^{N}U_k\Phi_k(X,Y),\quad V\approx\sum_{k=1}^{N}V_k\Phi_k(X,Y),\quad \text{and}\quad \theta\approx\sum_{k=1}^{N}\theta_k\Phi_k(X,Y) \tag{11}$$

for

$$0\le X,Y\le 1,$$

the system of equations for Eqs. (5), (9) and (10) along with boundary conditions are solved using Galerkin finite element method. The detailed solution procedure based on Galerkin finite element method [39] is discussed in an earlier work [40].

2.1. Streamfunction

The fluid motion is displayed using the streamfunction (ψ) obtained from the velocity components U and V. The relationships between the streamfunction and the velocity components for two-dimensional flows are

$$U=\frac{\partial\psi}{\partial Y}\ \text{and}\ V=-\frac{\partial\psi}{\partial X} \tag{12}$$

which yield a single equation

$$\frac{\partial^2\psi}{\partial X^2}+\frac{\partial^2\psi}{\partial Y^2}=\frac{\partial U}{\partial Y}-\frac{\partial V}{\partial X} \tag{13}$$

Using the above definition of the streamfunction, the positive sign of ψ denotes anti-clockwise circulation and the clockwise circulation is represented by the negative sign of ψ. The no-slip condition is valid at all boundaries and there is no cross flow, hence $\psi=0$ is used as residual equations at the nodes for the boundaries. Finally, streamfunctions (ψ) at various nodes are obtained via finite element post-processing as discussed in earlier work [40].

2.2. Entropy generation

In a natural convection system of non-isothermal flows of single-phase, viscous fluids without chemical reactions, the associated irreversibilities are due to heat transfer and fluid friction. According to the local thermodynamic equilibrium of linear transport theory [1], the dimensionless form of local entropy generation rate due to heat transfer (S_θ) and fluid friction (S_ψ) for

a two-dimensional heat and fluid flow in porous media in Cartesian coordinates in explicit form is written as:

$$S_\theta = \left[\left(\frac{\partial\theta}{\partial X}\right)^2+\left(\frac{\partial\theta}{\partial Y}\right)^2\right] \tag{14}$$

$$S_\psi = \phi\left\{\left[U^2+V^2\right]+Da\left[2\left(\left(\frac{\partial U}{\partial X}\right)^2+\left(\frac{\partial V}{\partial Y}\right)^2\right)+\left(\frac{\partial U}{\partial Y}+\frac{\partial V}{\partial X}\right)^2\right]\right\} \tag{15}$$

Note that, the viscous dissipation model as proposed by Al-Hadhrami et al. [41] is employed in Eq. (15). It may be noted that, there are three different models for viscous dissipation for flow through porous media. In a recent study, Hooman and Gurgenci [42] compared the three different viscous dissipation models and concluded that the three models are effectively same at low values of *Da* but for higher limits of *Da*, only the model of Al-Hadhrami et al. [41] is valid. A detailed discussion on different viscous dissipation models, their limits of applicability and other relevant issues on various aspects of modeling viscous dissipation in porous media may be found in earlier works [43,44].

It may be noted that, the effect of viscous dissipation is neglected in the energy equation (Eq. (5)), but that is considered for estimation of S_ψ. The condition when the viscous dissipation may be neglected in energy equation for natural convection systems is given by the condition, $Ge \ll 1$, where *Ge* is Gebhart number, defined as $Ge = g\beta L/c_p$. For various fluids such as molten metals, gases at ordinary temperatures, aqueous solutions, and the viscous fluids such as engine oils and silicones, the quantity $g\beta/c_p$ is very low ($\sim O(10^{-7}$–$10^{-10})$) and viscous dissipation effect can become significant only for a very large values of *L*, which is not encountered commonly [45]. Similar studies on entropy generation during natural convection in enclosures where viscous dissipation term is omitted in the energy equation are reported earlier [27,30].

In the expression for S_ψ (Eq. (15)), the parameter ϕ is called the irreversibility distribution ratio and it is defined as:

$$\phi = \frac{\mu T_o}{k}\left(\frac{\alpha_m^2}{K\Delta T^2}\right) \tag{16}$$

In the current study, ϕ is taken as 10^{-2}. An order of magnitude analysis would also give a similar result. For example, the properties for air at 298 K are in the range of $\mu \sim O(10^{-5})$, $k \sim O(10^{-2})$, $\alpha_m \sim O(10^{-5})$, $K \sim O(10^{-12})$ and for a representative case with $\Delta T^2/T_o \sim O(10^2)$, ϕ is obtained as $O(10^{-2})$. Here, T_o is the bulk temperature, evaluated as $(T_h + T_c)/2$. A similar value of ϕ was considered by earlier researchers [30].

It may be noted that, the accurate evaluation of derivatives is necessary for estimation of S_θ and S_ψ. Small error in calculation of temperature and velocity gradients would propagate to a much larger error since the derivatives are powered to 2. As mentioned earlier, the derivatives are evaluated based on finite element method in this work. Current approach offers special advantage over finite difference or finite volume solutions [27,30] where derivatives are calculated using some interpolation functions which are avoided in the current work and elemental basis set are used to estimate S_θ and S_ψ. The derivative of any function *f* over an element *e* is written as

$$\frac{\partial f^e}{\partial n} = \sum_{k=1}^{9} f_k^e \frac{\partial \Phi_k^e}{\partial n} \tag{17}$$

where, $f_k{}^e$ is the value of the function at local node *k* in the element *e* and $\Phi_k{}^e$ is the elemental basis function. There are nine sets of basis functions for a bi-quadratic element. Further, since each node is shared by four elements (in the interior domain) or two elements (along the boundary), the value of the derivative of any function at the global node number (*i*), is averaged over those shared elements (N^e), i.e.,

$$\frac{\partial f_i}{\partial n} = \frac{1}{N^e}\sum_{e=1}^{N^e}\frac{\partial f_i^e}{\partial n} \tag{18}$$

Therefore, at each node, local entropy generation for thermal ($S_{\theta,i}$) and flow fields ($S_{\psi,i}$) are given by,

$$S_{\theta,i} = \left[\left(\frac{\partial\theta_i}{\partial X}\right)^2+\left(\frac{\partial\theta_i}{\partial Y}\right)^2\right] \tag{19}$$

$$S_{\psi,i} = \phi\left\{\left[U_i^2+V_i^2\right]+Da\left[2\left(\frac{\partial U_i}{\partial X}\right)^2+2\left(\frac{\partial V_i}{\partial Y}\right)^2+\left(\frac{\partial U_i}{\partial Y}+\frac{\partial V_i}{\partial X}\right)^2\right]\right\} \tag{20}$$

Note that, the derivatives, $\partial\theta_i/\partial X, \partial\theta_i/\partial Y, \partial U_i/\partial X, \partial U_i/\partial Y, \partial V_i/\partial X$ and $\partial V_i/\partial Y$ are evaluated following Eq. (18). The combined total entropy generation (S_{total}) in the cavity is given by the summation of total entropy generation due to heat transfer ($S_{\theta,total}$) and fluid friction ($S_{\psi,total}$), which in turn are obtained via integrating the local entropy generation rates (S_θ and S_ψ) over the domain Ω.

$$S_{total} = \int_\Omega S_\theta d\Omega + \int_\Omega S_\psi d\Omega = S_{\theta,total} + S_{\psi,total} \tag{21}$$

where,

$$S_{\theta,total} = \int_\Omega\left\{\left[\frac{\partial}{\partial X}\left(\sum_{k=1}^{N}\theta_k\Phi_k\right)\right]^2+\left[\frac{\partial}{\partial Y}\left(\sum_{k=1}^{N}\theta_k\Phi_k\right)\right]^2\right\}d\Omega \tag{22}$$

$$\begin{aligned} S_{\psi,total} = \phi\int_\Omega\Bigg\{&\left[\left(\sum_{k=1}^{N}U_k\Phi_k\right)\right]^2+\left[\left(\sum_{k=1}^{N}V_k\Phi_k\right)\right]^2 \\ &+Da\left(2\left[\frac{\partial}{\partial X}\left(\sum_{k=1}^{N}U_k\Phi_k\right)\right]^2+2\left[\frac{\partial}{\partial Y}\left(\sum_{k=1}^{N}V_k\Phi_k\right)\right]^2\right) \\ &+\left[\frac{\partial}{\partial Y}\left(\sum_{k=1}^{N}U_k\Phi_k\right)+\frac{\partial}{\partial X}\left(\sum_{k=1}^{N}V_k\Phi_k\right)^2\right]\Bigg\}d\Omega \end{aligned} \tag{23}$$

The integrals are evaluated using three point Gaussian quadrature integration method. The relative dominance of entropy generation due to heat transfer and fluid friction is given by average Bejan number (Be_{av}), a dimensionless parameter defined as,

$$Be_{av} = \frac{S_{\theta,total}}{S_{\theta,total}+S_{\psi,total}} = \frac{S_{\theta,total}}{S_{total}} \tag{24}$$

Therefore, $Be_{av} \gg 0.5$ implies the dominance of heat transfer irreversibility and $Be_{av} \ll 0.5$ implies the dominance of fluid friction irreversibility.

2.3. Cup-mixing temperature and temperature uniformity

In order to compare the thermal mixing in various cases, the bulk average temperature across the cavity, i.e., 'cup-mixing temperature' is defined. Cup-mixing temperature is the velocity–weighted

Table 1
Comparison of the present results with the benchmark solutions of earlier works for natural convection in a porous square cavity with air ($Pr = 0.71$) as fluid medium at $Ra_m = Ra \times Da = 1000$. Present study employs 28×28 bi-quadratic elements (57×57 grid points).

References	$\overline{Nu}$
Bejan [46]	15.800
Manole and Lage [47]	13.637
Saeid and Pop [25]	13.726
Baytas and Pop [48]	14.060
Present work	14.165

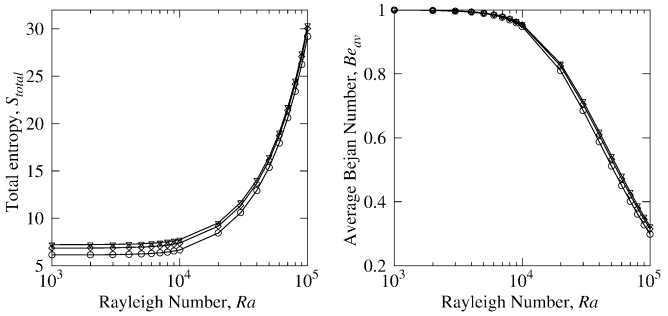

Fig. 2. Variation of total entropy generation (S_{total}) and average Bejan number (Be_{av}) with Ra for a clear-fluid case in case 2 for $Pr = 1000$ for different mesh sizes 20×20 (○), 24×24 (◇) and 28×28 (▽) bi-quadratic elements, which correspond to 41×41, 49×49 and 57×57 grid points, respectively.

average temperature, and it is most suitable when convective flow exists. The cup-mixing temperature (Θ_{cup}) and spatial average or area average temperature (Θ_{avg}) are given as

$$\Theta_{cup} = \frac{\int\int \hat{V}(X,Y)\theta(X,Y)\mathrm{d}X\mathrm{d}Y}{\int\int \hat{V}(X,Y)\mathrm{d}X\mathrm{d}Y} \tag{25}$$

where

$$\hat{V}(X,Y) = \sqrt{U^2+V^2}$$

and

$$\Theta_{avg} = \frac{\int\int \theta(X,Y)\mathrm{d}X\mathrm{d}Y}{\int\int \mathrm{d}X\mathrm{d}Y} \tag{26}$$

Further, 'root-mean square deviation (RMSD)' is defined to quantify the degree of temperature uniformity in each case. Various forms of RMSDs are defined based on cup-mixing temperature (Θ_{cup}) and spatial average temperature (Θ_{avg}) as follows:

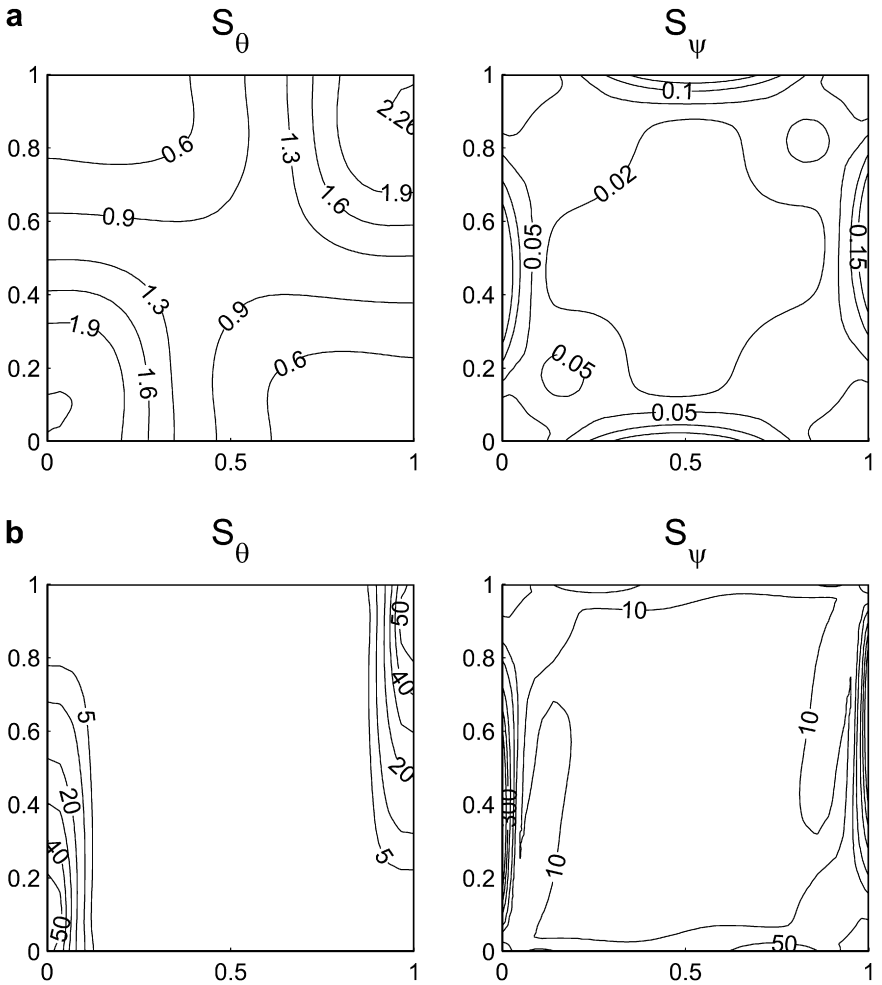

Fig. 3. Local entropy generation due to heat transfer ($S_{\theta,i}$) and fluid friction ($S_{\psi,i}$) for cavity with hot left wall and cold right wall with adiabatic top and bottom walls at (a) $Ra = 10^3$ (b) $Ra = 10^5$ for $Pr = 0.7$ (benchmark problem).

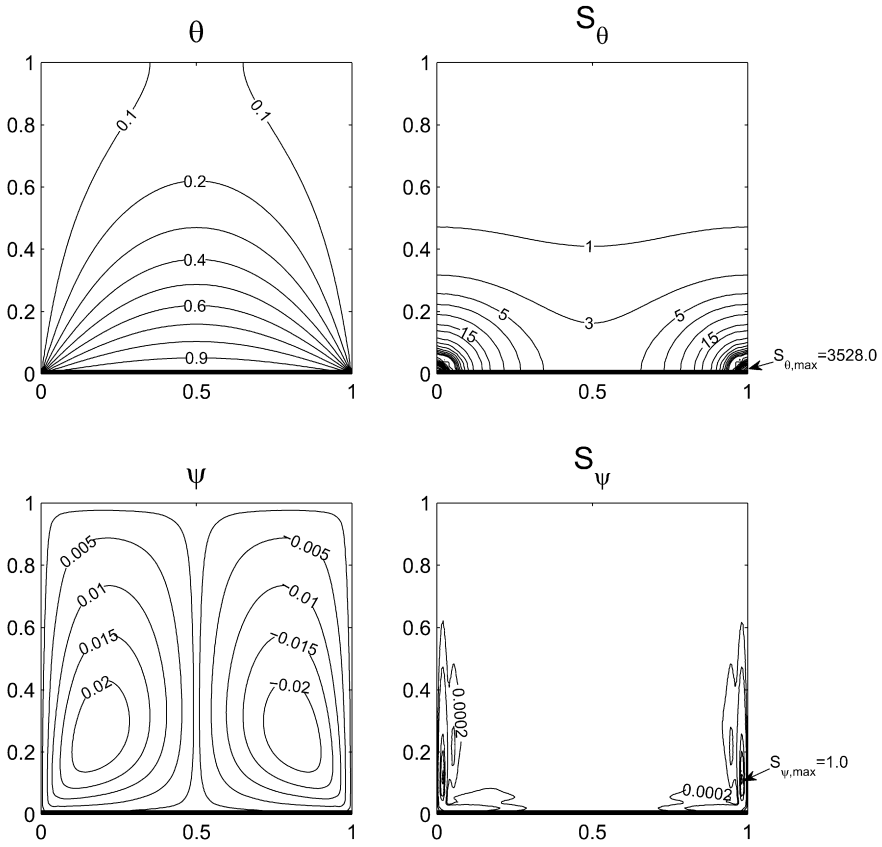

Fig. 4. Isotherms (θ), streamlines (ψ), local entropy generation due to heat transfer ($S_{\theta,i}$) and entropy generation due to fluid friction ($S_{\psi,i}$) contours for case 1 with $Pr = 0.015$, $Da = 10^{-6}$ and $Ra = 10^{6}$.

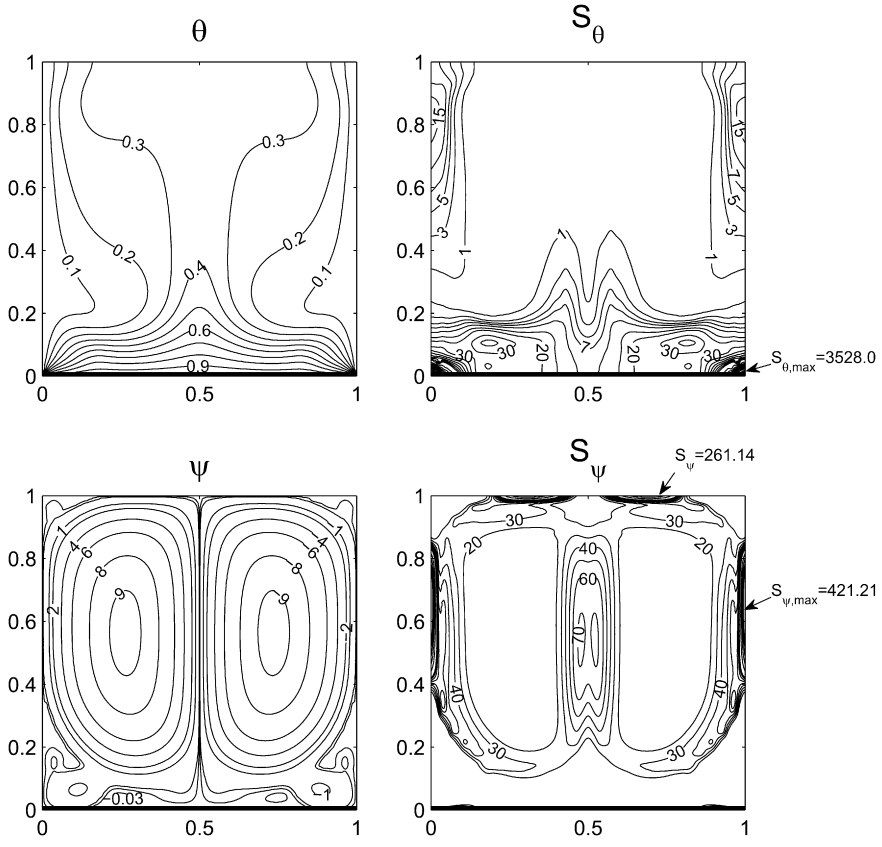

Fig. 5. Isotherms (θ), streamlines (ψ), local entropy generation due to heat transfer ($S_{\theta,i}$) and entropy generation due to fluid friction ($S_{\psi,i}$) contours for case 1 with $Pr = 0.015$, $Da = 10^{-3}$ and $Ra = 10^{6}$.

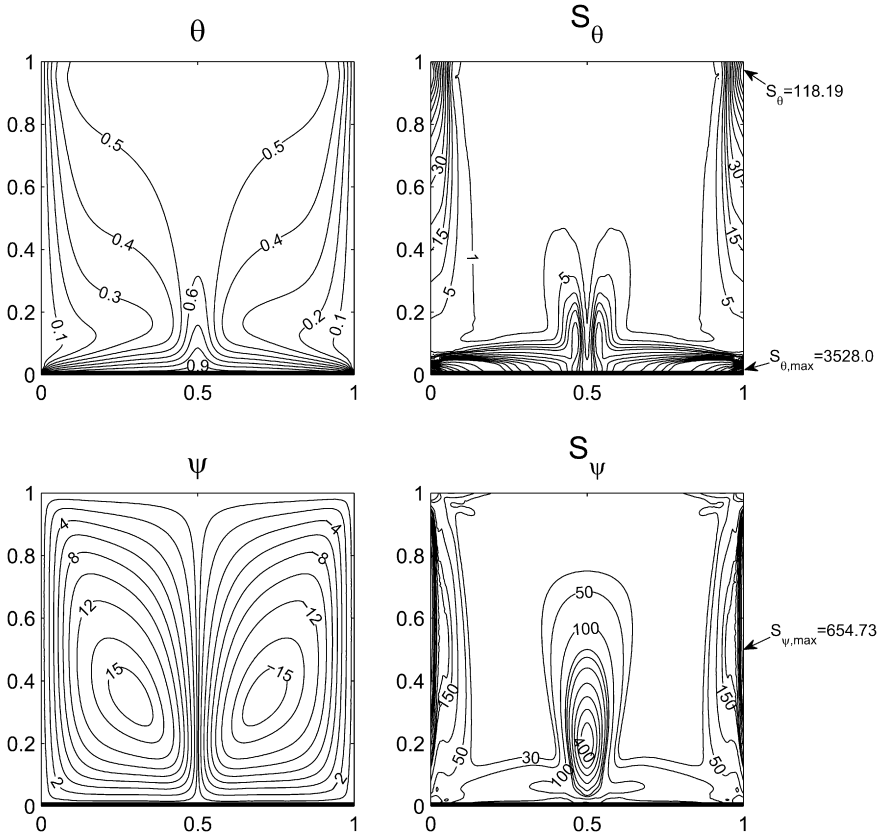

Fig. 6. Isotherms (θ), streamlines (ψ), local entropy generation due to heat transfer ($S_{\theta,i}$) and entropy generation due to fluid friction ($S_{\psi,i}$) contours for case 1 with $Pr = 1000$, $Da = 10^{-3}$ and $Ra = 10^6$.

$$\mathrm{RMSD}_{\Theta_{\mathrm{cup}}} = \sqrt{\frac{\sum_{i=1}^{N}\left(\theta_i - \Theta_{\mathrm{cup}}\right)^2}{N}} \tag{27}$$

and

$$\mathrm{RMSD}_{\Theta_{\mathrm{avg}}} = \sqrt{\frac{\sum_{i=1}^{N}\left(\theta_i - \Theta_{\mathrm{avg}}\right)^2}{N}} \tag{28}$$

It may be noted that, the lower values of RMSD indicate higher temperature uniformity in the cavity and vice-versa. In addition, RMSD cannot exceed 1 as the dimensionless temperature varies only between 0 and 1.

3. Results and discussion

3.1. Numerical procedure and validation

The computational domains consisting of 20 × 20, 24 × 24 and 28 × 28 bi-quadratic elements, which correspond to 41 × 41, 49 × 49 and 57 × 57 grid points, respectively are considered for the study. For discrete heating situations, jump discontinuities exist at the edges of the discrete heat sources which correspond to mathematical singularities. The problem is resolved by specifying the average temperature of the two walls at the hot–cold junction points and keeping the adjacent grid–nodes at the respective wall temperatures. Gaussian quadrature based finite element method has been used in current investigation and this method provides smooth solutions in the computational domain including the singular points as evaluation of residuals depends on interior Gauss points. In addition, it is ensured that the overall heat balance is satisfied. The heat balance equation for each case may be written as

(i) Case 1:

$$\overline{Nu_{\mathrm{b}}} = \overline{Nu_{\mathrm{b}}} = \overline{Nu_{\mathrm{l}}} + \overline{Nu_{\mathrm{r}}} \tag{29}$$

(ii) Case 2:

$$l'_{\mathrm{b},2}\overline{Nu_{\mathrm{b},2}} + l'_{\mathrm{l},2}\overline{Nu_{\mathrm{l},2}} + l'_{\mathrm{r},2}\overline{Nu'_{\mathrm{r},2}} = l'_{\mathrm{b},1}\overline{Nu_{\mathrm{b},1}} + l'_{\mathrm{b},3}\overline{Nu_{\mathrm{b},3}} + l'_{\mathrm{l},1}\overline{Nu_{\mathrm{l},1}} + l'_{\mathrm{l},3}\overline{Nu_{\mathrm{l},3}} + l'_{\mathrm{r},1}\overline{Nu_{\mathrm{r},1}} + l'_{\mathrm{r},3}\overline{Nu_{\mathrm{r},3}} \tag{30}$$

(iii) Case 3:

$$l'_{\mathrm{b},1}\overline{Nu_{\mathrm{b},1}} + l'_{\mathrm{b},3}\overline{Nu_{\mathrm{b},3}} + l'_{\mathrm{b},5}\overline{Nu_{\mathrm{b},5}} + l'_{\mathrm{l},1}\overline{Nu_{\mathrm{l},1}} + l'_{\mathrm{l},3}\overline{Nu_{\mathrm{l},3}} + l'_{\mathrm{r},1}\overline{Nu'_{\mathrm{r},1}} + l'_{\mathrm{r},3}\overline{Nu'_{\mathrm{r},3}} = l'_{\mathrm{b},2}\overline{Nu_{\mathrm{b},2}} + l'_{\mathrm{b},4}\overline{Nu_{\mathrm{b},4}} + l'_{\mathrm{l},2}\overline{Nu_{\mathrm{l},2}} + l'_{\mathrm{l},4}\overline{Nu_{\mathrm{l},4}} + l'_{\mathrm{r},2}\overline{Nu_{\mathrm{r},2}} + l'_{\mathrm{r},4}\overline{Nu_{\mathrm{r},4}} \tag{31}$$

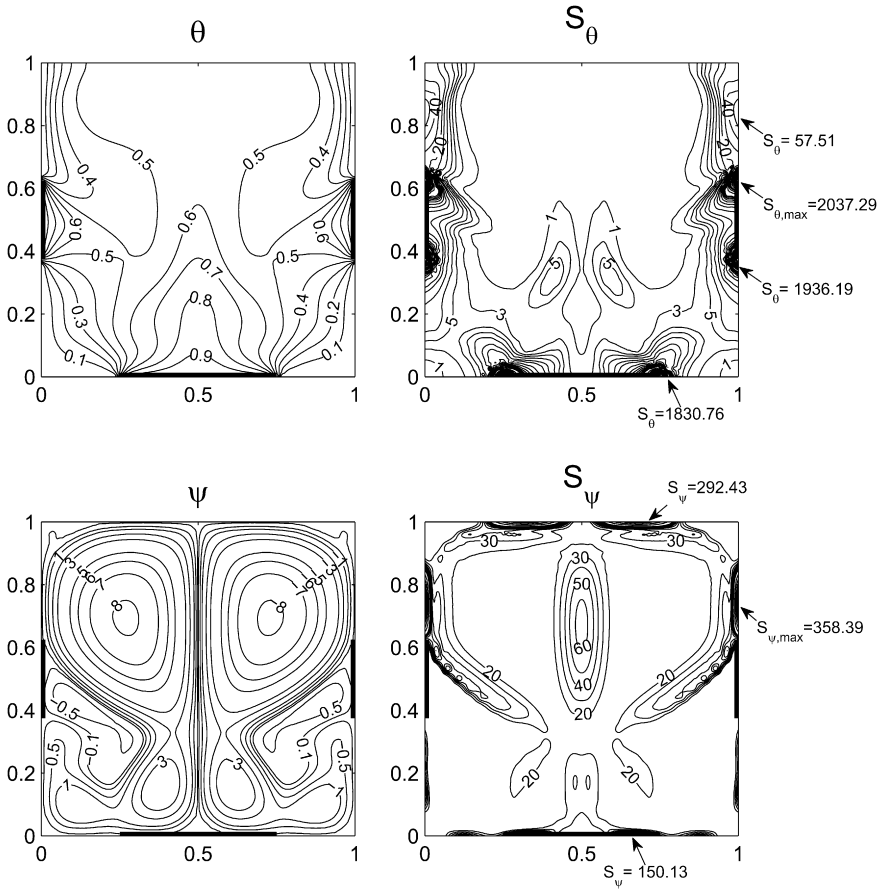

Fig. 7. Isotherms (θ), streamlines (ψ), local entropy generation due to heat transfer ($S_{\theta,i}$) and entropy generation due to fluid friction ($S_{\psi,i}$) contours for case 2 with $Pr = 0.015$, $Da = 10^{-3}$ and $Ra = 10^6$.

The error in heat balance is calculated as:

$$\epsilon = \frac{\left|\sum_{m=1}^{N_h} l'_{j,m}\overline{Nu_{j,m}}\right|_{\text{hot}} - \left|\sum_{m=1}^{N_c} l'_{j,m}\overline{Nu_{j,m}}\right|_{\text{cold}}}{\min\left(\left|\sum_{m=1}^{N_h} l'_{j,m}\overline{Nu_{j,m}}\right|_{\text{hot}}, \left|\sum_{m=1}^{N_c} l'_{j,m}\overline{Nu_{j,m}}\right|_{\text{cold}}\right)} \times 100 \qquad (32)$$

where $\overline{Nu}$ is the average Nusselt number, l' refers to length of cold or hot sections, j refers to left (l), bottom (b) and right (r) walls. Subscripts $m = 1,3$ (cold sections) and 2 (hot section) on each wall in case 2 whereas in case 3, $m = 1,3,5$ (hot sections) and 2, 4 (cold sections) and N_h and N_c refer to the total number of hot and cold sections in the cavity for given case respectively. For each case, it is ensured that the error is less than 1% across the range of Da.

Further, the present numerical procedure is validated for a porous medium case where a porous square cavity, with air ($Pr = 0.71$) as fluid, is heated isothermally on the left wall while the right wall is maintained cold isothermal and the horizontal walls are maintained adiabatic, similar to the problem reported by Bejan [46], Manole and Lage [47], Saeid and Pop [25] and Baytas and Pop [48]. The comparison of average Nusselt number with the results reported earlier at modified Rayleigh number, $Ra_m = 1000$, where $Ra_m = Ra \times Da$, are presented in Table 1. It may be noted that the error between the average Nusselt number obtained by current numerical procedure is only 0.74% compared to the one reported by Baytas and Pop [48].

Due to unavailability of studies on entropy generation for natural convection flow within fluid-saturated porous medium, the proposed numerical scheme has been validated with the entropy generation due to natural convection for a clear-fluid case. Fig. 2 depicts the mesh convergence studies for case 2 (Fig. 1(b)) filled with clear-fluid. It is found that the values of S_{total} and Be_{av} obtained from 49×49 and 57×57 mesh at high Ra are within 1%, and thus, 57×57 mesh has also been found to be adequate for all case studies as shown in Fig. 1(a)–(c). It may be noted that the S_ψ formulation for clear-fluid is different from that of porous medium case (Eq. (20)) and that can be found in earlier work [49]. Using 57×57 mesh, the benchmark studies for entropy generation were carried out for a differentially heated square cavity filled with clear-fluid with hot left wall and cold right wall in the presence of adiabatic top and bottom walls, similar to the case reported by Ilis et al. [49]. The results in terms of streamlines, isotherms, entropy generation due to heat transfer and fluid friction are in excellent agreement with the earlier work [49] (see Fig. 3).

Detailed computations have been carried out for various fluids of Pr ($Pr = 0.015$, 0.7, 10, 1000) within $Da = 10^{-6}$–10^{-3} and $Ra = 10^3$–10^6 for different cases and they are discussed below.

3.2. Case 1

The schematic diagram of this case is shown in Fig. 1(a). The bottom wall of the cavity is maintained hot isothermal while the vertical walls are maintained cold isothermal and the top wall is adiabatic. At low $Da(10^{-6})$ and $Pr = 0.015$, the permeability of the porous medium is low and therefore the resistance to fluid flow is

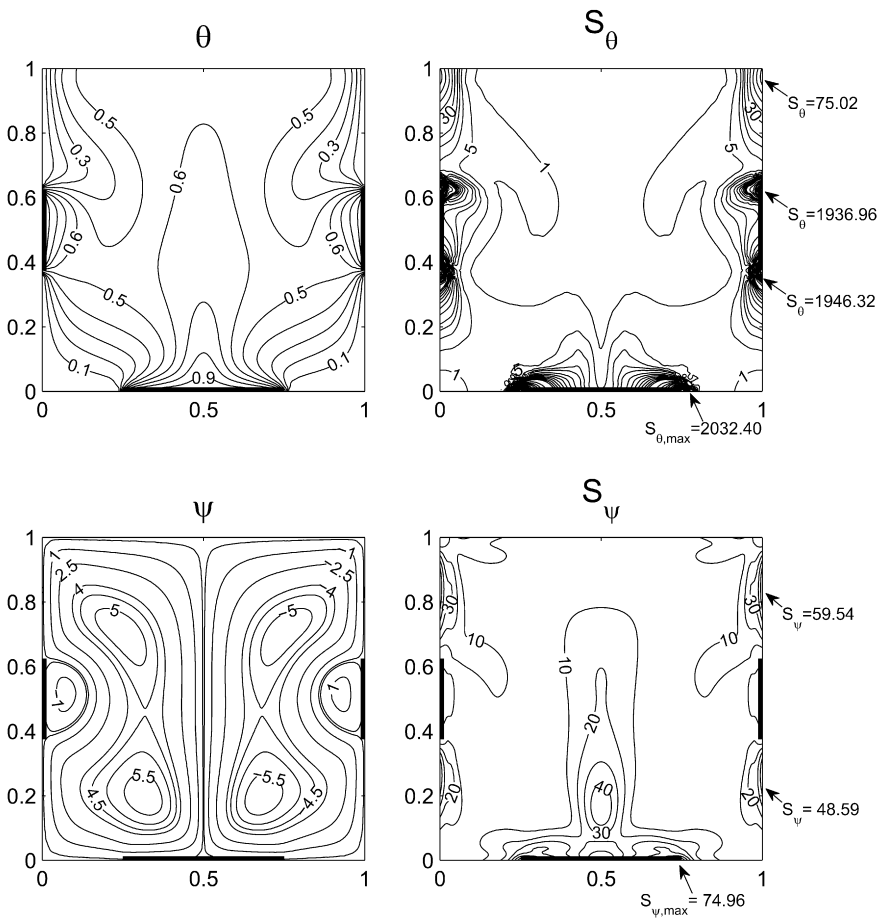

Fig. 8. Isotherms (θ), streamlines (ψ), local entropy generation due to heat transfer ($S_{\theta,i}$) and entropy generation due to fluid friction ($S_{\psi,i}$) contours for case 2 with $Pr = 1000$, $Da = 3.3 \times 10^{-4}$ and $Ra = 10^6$.

high. Consequently, the fluid flow is weak as seen from the magnitudes of streamfunctions (see Fig. 4). High thermal gradients are concentrated at the lower corner regions where the singularity exists and hence the entropy generation due to heat transfer (S_θ) is found to be very high at the lower corners with a local maxima, $S_{\theta,\max} = 3528$. Note that, the S_θ extends upto the central region, influencing nearly the half-area of the cavity. In contrast, due to weak fluid velocities, the frictional irreversibility is low and hence the entropy generation due to fluid friction (S_ψ) is found to be insignificant compared to S_θ with $S_{\psi,\max} = 1$.

As Da increases to 10^{-3}, the permeability of the porous medium is increased and thus the fluid flow is intense resulting in enhanced convective transport of heat from the bottom wall. Therefore, the thermal gradients extend over the entire length of the bottom wall as seen from the compression of isotherms (see Fig. 5). The corresponding entropy generation due to heat transfer is found to extend over the bottom wall, with $S_{\theta,\max} = 3528$ at the corner regions. It may be noted that the contours of S_θ are highly dense at lower corners compared to the central zone near the bottom wall due to larger thermal gradients at singular points. The enhanced buoyancy driven flow transfers large amount of heat to the upper cold portions of side walls and that results in thin thermal boundary layer and therefore, $S_\theta \leq 15$ is observed at those regions. Enhanced fluid circulation further leads to increased S_ψ along the top and side walls of the cavity. High velocity gradients are induced near the walls due to strong fluid flow resulting in global $S_{\psi,\max} = 421.21$ on the side walls. In addition, the higher magnitudes of S_ψ are also observed in the interior regions of the cavity due to velocity gradients near the walls and due to the friction between the counter rotating circulation cells along the vertical center line with a local $S_{\psi,\max} = 70$. It is interesting to note that, the adiabatic top wall acts as an active site for S_ψ with a local maximum of 261.14 while S_ψ along the bottom wall is observed to be negligible (see Fig. 5). This is due to the fact that the secondary circulation cells of smaller magnitudes gradually develop near the bottom wall and that further reduces the fluid friction along the bottom wall. It will be shown later that the total entropy generation (S_{total}) in the cavity is influenced by these weak secondary circulation cells.

As Pr increases to 1000 (Fig. 6), convection is further enhanced in the cavity due to high momentum diffusivity of high Pr fluid. The local $S_{\theta,\max}$ is found to be 118.19 near the top corners, while the global maximum is observed near the lower corners. Note that, dense contours of S_θ are observed along the bottom wall indicating high entropy generation due to high thermal gradients. The thermal boundary layer extends upto $Y = 0.2$ and S_θ occurs along a large region of the side walls. The side walls also act as strong active sites of S_ψ with a maximum magnitude of 654.73 near the central zones. The frictional irreversibility at the lower central region of the cavity is found to be $S_\psi = 400$ due to friction between counter rotating circulation cells. It may be noted that the magnitudes of S_ψ at all regions are significantly higher compared to that in $Pr = 0.015$ case as the fluid circulation is stronger for higher Pr with $|\psi|_{\max} = 15$. It is interesting to note that, in contrast to that in lower Pr case, the top wall does not contribute any S_ψ as the circulation cells are skewed diagonally in each vertical half of the cavity which minimizes the velocity gradients along the top wall

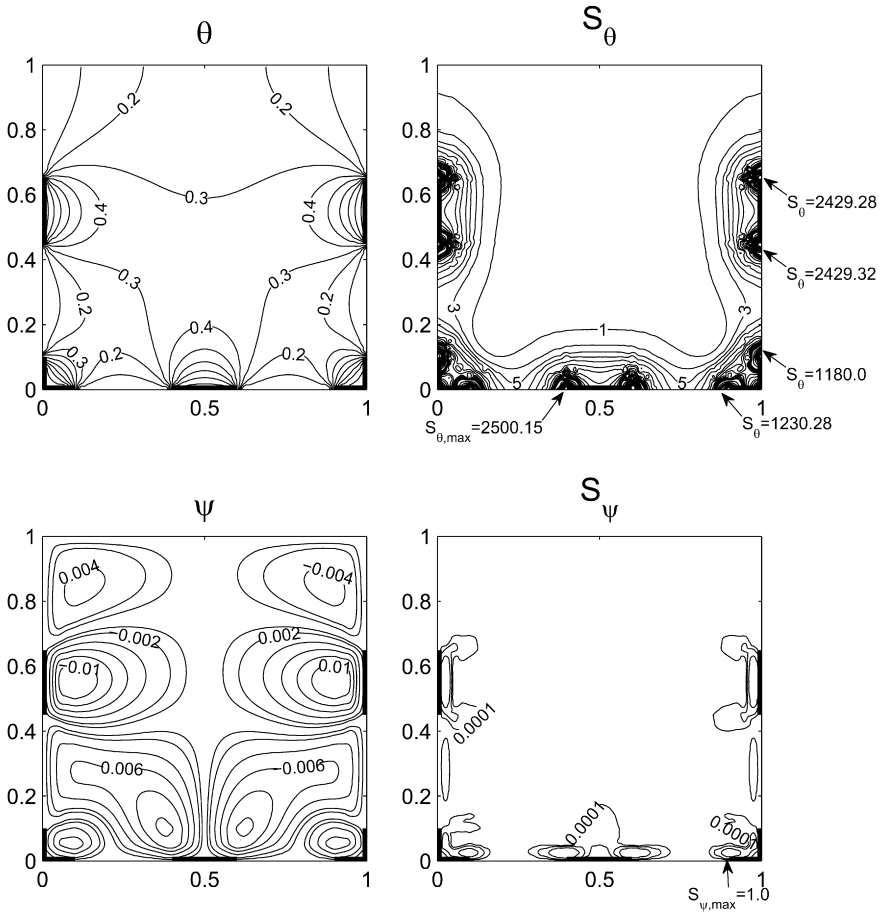

Fig. 9. Isotherms (θ), streamlines (ψ), local entropy generation due to heat transfer ($S_{\theta,i}$) and entropy generation due to fluid friction ($S_{\psi,i}$) contours for case 3 with $Pr = 0.015$, $Da = 10^{-6}$ and $Ra = 10^6$.

(see Fig. 6). The qualitative features of S_θ and S_ψ are found to be nearly similar for $Pr = 0.7$ and 10 cases and hence those results are not shown for brevity.

It may be noted from the above analysis that a thermal processing methodology based on differential heating of porous cavity results in large entropy generation. In order to reduce the exergy loss due to thermal and fluid irreversibilities, a distributed heating methodology is proposed, wherein the porous medium saturated with fluid is heated with multiple discrete heat sources along the walls of the cavity. Two different cases are considered where the cavity is heated with three and seven discrete heat sources respectively, which are placed at the strategic locations. The total dimensionless length of the discrete heat sources in both the cases is maintained same as that in the differentially heated cavity (case 1). A detailed study on entropy generation in porous cavities due to distributed heating methodology is discussed in the following sections.

3.3. Case 2

This case refers to the distributed heating case where the cavity is heated with three discrete heat sources as depicted in Fig. 1(b)). The distributed heating resulted in $\theta = 0.4$–0.5 at the core even at low Da (figure not shown). The entropy generation due to heat transfer was found to be concentrated near the edges of the heat sources with $S_{\theta,\max} \approx 1936$, which was about 46% reduction compared to the $S_{\theta,\max}$ in case 1. The entropy due to fluid friction irreversibility is observed to be negligible at low Da as the hydraulic resistance of the porous medium is high. As Da increases to 10^{-3}, multiple circulations are observed in the cavity due to discrete heat sources (Fig. 7). As the permeability of porous media is increased, the heat flow from each of the three heat sources is also enhanced. Entropy generation due to heat transfer is observed along a large portion of the side walls with $S_{\theta,\max} = 2037.29$ near the upper edges of the heat sources of the side walls. The thermal gradients at the central core also result in $S_\theta = 5$, but the upper core region is maintained as nearly entropy free region due to enhanced thermal mixing that results in the uniform temperature of the fluid within $\theta = 0.5$–0.6. The entropy generation due to fluid friction is observed along the upper portion of the side walls, and in the interior region, at the interface of the counter rotating circulation cells. It may be noted that the active region for S_ψ is reduced and that spans only within $0.65 \leq Y \leq 0.85$ along the side walls whereas the active region spans a larger region within $0.42 \leq Y \leq 0.85$ in case 1 for identical Da, Pr and Ra. Further, it is observed that $S_{\psi,\max}$ is reduced (=358.39) compared to that in case 1.

Fig. 8 illustrates the isotherms, streamlines and entropy generation maps due to heat transfer and fluid friction at $Da = 3.3 \times 10^{-4}$, $Ra = 10^6$ for $Pr = 1000$. The significance of this Da is that the magnitudes of entropy generation due to heat transfer irreversibility (S_θ) and fluid friction irreversibility (S_ψ) are equal and therefore S_{total} in the cavity is equally dominated by S_θ and S_ψ. This critical Da corresponds to the average Bejan number (Be_{av}) of 0.5, obtained from Be_{av} vs Da plot shown in Fig. 12(d). The thermal gradients are developed near the cold upper region of the cavity and a local maximum of $S_\theta = 75.02$ is observed at that region. The

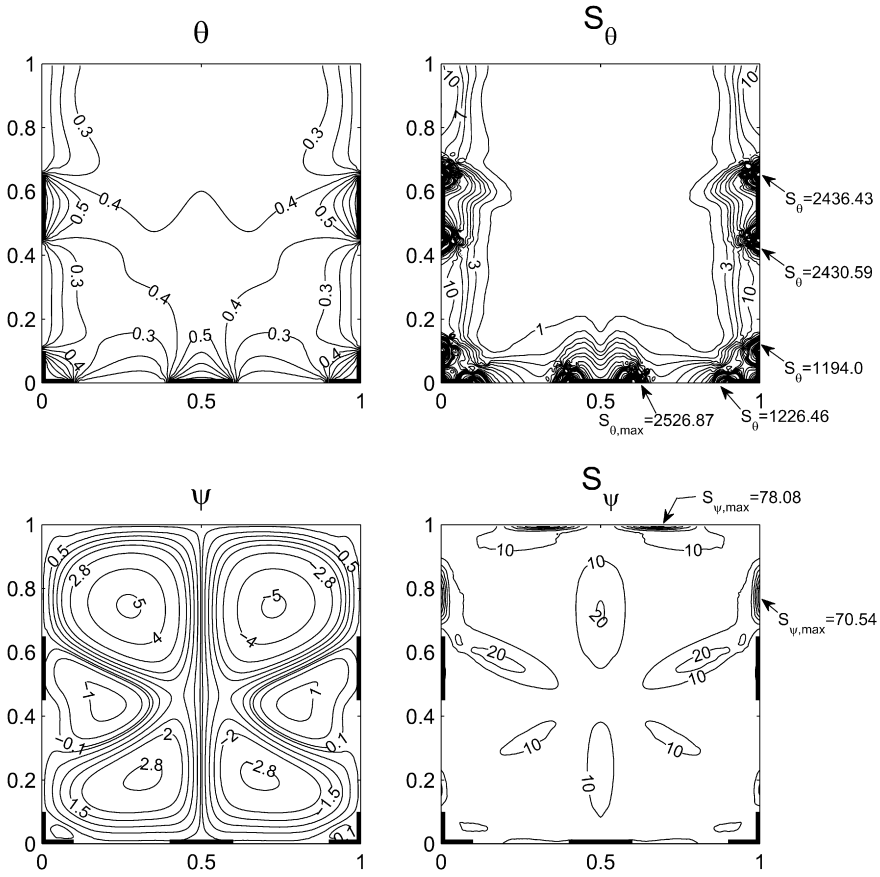

Fig. 10. Isotherms (θ), streamlines (ψ), local entropy generation due to heat transfer ($S_{\theta,i}$) and entropy generation due to fluid friction ($S_{\psi,i}$) contours for case 3 with $Pr = 0.015$, $Da = 10^{-3}$ and $Ra = 10^6$.

global maxima of S_θ is observed near the hot-cold junctions of the bottom wall with $S_{\theta,\max} = 2032.40$ in addition to the local maxima at the hot–cold junctions of the side walls with $S_\theta = 1936.96$ and 1946.32, respectively. Similar to the S_θ, a high frictional irreversibility is observed near the bottom wall ($S_{\psi,\max} = 74.96$) as the eye of the primary vortex occurs at the lower portion of the cavity. The velocity gradients induced by the strong primary circulation lead to the entropy production at the upper and lower cold regions of the side walls. On the other hand, S_ψ due to secondary circulation is observed near the heat sources of the side walls and in the interior region with $S_\psi = 10$. As Da increases to 10^{-3} (figure not shown), the enhanced convection leads to the further increment of the temperature and velocity gradients and therefore the local entropy generation rate is also increased significantly.

3.4. Case 3

In this case, the heat sources are further divided into smaller sections and they are placed at strategic locations in the cavity (see Fig. 1(c)). It may be noted that the bulk of the fluid is retained cold in the lower corner regions for case 2 (see Figs. 7 and 8). Therefore, the heat sources are placed at those corners and the analysis on the entropy generation has been carried out. Fig. 9 shows the distributions for θ, ψ, S_θ and S_ψ for $Da = 10^{-6}$, $Pr = 0.015$ at $Ra = 10^6$. It is observed that the temperature at the core region is maintained uniformly within in 0.3–0.4 even when the thermal mixing is weak at low permeability of porous medium. Therefore, the magnitude of S_θ and S_ψ are found to be negligible at low Da.

As Da increases to 10^{-3} (Fig. 10), multiple circulations are observed in the cavity for the fluid with $Pr = 0.015$. Due to enhanced thermal mixing by the multiple circulation cells the temperature in the interior region is maintained uniformly within $\theta = 0.3$–0.5. Consequently, the thermal gradients are low and the entropy generation due to heat transfer (S_θ) is observed to be negligible in the central core region. High values of S_θ occur near the hot-cold junctions with $S_{\theta,\max} = 2526.87$ along the bottom wall. It may be noted that, the $S_{\theta,\max}$ is higher than that in case 2 due to enhanced heat transfer rate in case 3. It is interesting to note the entropy generation due to fluid friction (S_ψ) in this case. A remarkable reduction in S_ψ is observed, as seen from the sparsely occurring contours of S_ψ with small magnitudes. The frictional irreversibility at the walls is contributed significantly by the primary circulation cells where the global maximum of S_ψ ($S_{\psi,\max} = 78.08$) is observed at the top wall. Note that, the global $S_{\psi,\max}$ is reduced significantly by about 81.4% and 78.2% compared to those in cases 1 and 2, respectively, for identical parameters. Further, the entropy generation due to the friction between the circulation cells in the interior region of the cavity is also found to be low with local $S_{\psi,\max} = 20$.

At larger Pr ($Pr = 1000$), with $Da = 10^{-3}$ and $Ra = 10^6$ (see Fig. 11) the strength of all circulation cells are found to be increased and the primary circulation cells occur at the lower portion with $|\psi|_{max} = 6.5$. The qualitative features of local distribution of S_θ are observed to be similar to that for $Pr = 0.015$ except that the S_θ is enhanced near the hot–cold junctions due to enhanced heat transfer by the stronger secondary circulation cell with $|\psi|_{\max} = 3$. The global maximum value of S_θ is also increased to 2695.34 with the increase in Pr. The entropy generation due to fluid friction is confined to a small regime near the side walls and at the central lower region. It is found that S_ψ is significantly lower compared to

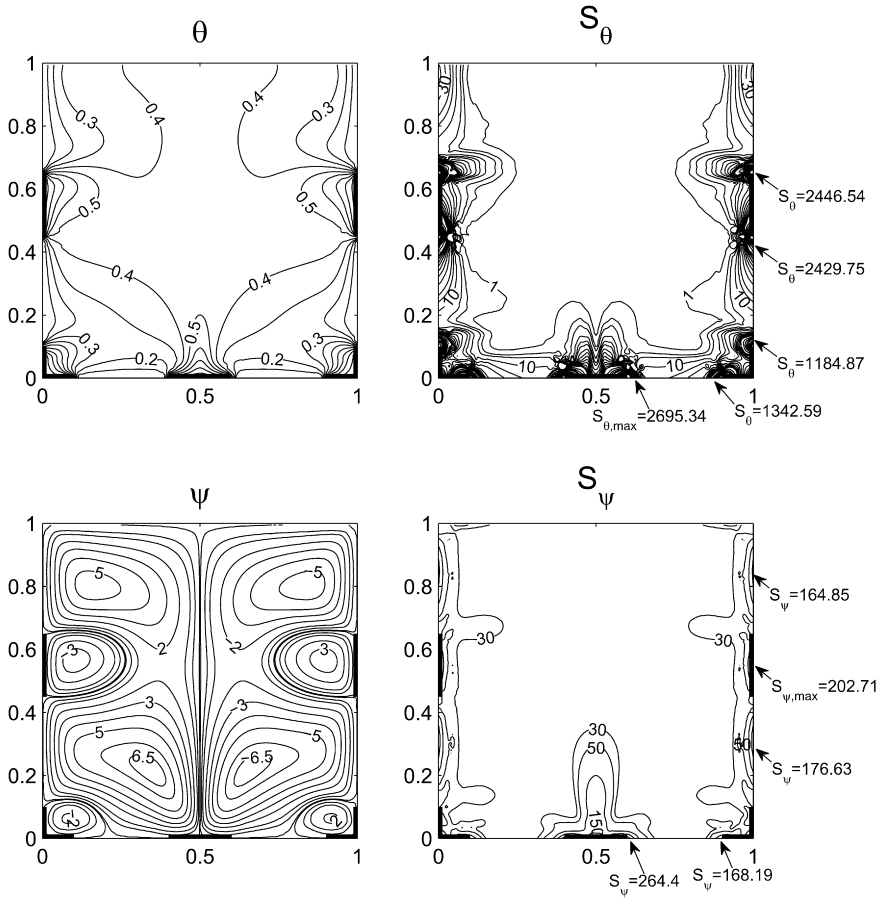

Fig. 11. Isotherms (θ), streamlines (ψ), local entropy generation due to heat transfer ($S_{\theta,i}$) and entropy generation due to fluid friction ($S_{\psi,i}$) contours for case 3 with $Pr = 1000$, $Da = 10^{-3}$ and $Ra = 10^6$.

that in case 1 (Fig. 6) and case 2 (figure not shown). Note that, $S_{\psi,\max} = 264.4$ and that is found to be 59.6% and 39.4% lesser compared to those in cases 1 and 2, respectively.

Analysis of local maps of entropy generation due to heat transfer and fluid friction in various cases indicates that the distributed heating methodology significantly lowers the entropy generation in the cavity and the intensity of S_θ and S_ψ at the local active sites is reduced. In the following section, a detailed discussion on total entropy generation (S_{total}) in various cases, the average Bejan number (Be_{av}), the thermal mixing and the temperature uniformity in various cases are presented.

3.5. Total entropy generation, average Bejan number, cup-mixing temperature and temperature uniformity

The three cases are analyzed for the role of total entropy generation (S_{total}) on overall heating effects within the cavity for $10^{-6} \le Da \le 10^{-3}$ at $Ra = 10^6$. The variation of S_{total} at $Da = 10^{-6}$ is found to be same as that at $Da = 10^{-5}$ and hence the variations are shown only for $Da = 10^{-5}$–10^{-3} in Fig. 12(a) and (b) ($Pr = 0.015$ and 0.7) and Fig. 13 (a) and (b) ($Pr = 10$ and 1000). Further, the variation of average Bejan number (Be_{av}) with Da is also shown. Note that the variation of Be_{av} indicates the dominance of S_θ or S_ψ. For, $Be_{\text{av}} \gg 0.5$, the total entropy generation in the cavity is dominated by heat transfer irreversibility while $Be_{\text{av}} \ll 0.5$ indicates that the total entropy generation is dominated by fluid friction irreversibility. The cup-mixing temperature (Θ_{cup}; Eq. (27)) is evaluated in order to analyze the thermal mixing in different configurations of the cavity during the convective flow. The degree of temperature uniformity in various cases is compared by the root-mean square deviation based on the cup-mixing temperature ($\text{RMSD}_{\Theta_{\text{cup}}}$; Eq. (27)) and the average temperature ($\text{RMSD}_{\Theta_{\text{avg}}}$; Eq. (28)) and they are presented in the lower panels of Figs. 12(a) and (b) and 13(a) and (b). As mentioned earlier, higher values of Θ_{cup} indicate the higher overall heating rate. On the other hand, the lower values of $\text{RMSD}_{\Theta_{\text{cup}}}$ or $\text{RMSD}_{\Theta_{\text{avg}}}$ indicate greater temperature uniformity within the cavity.

In general, the values of S_θ are order of magnitudes larger than S_ψ, and Be_{av} is an indicator to govern whether irreversibilities due to fluid flow are important. A smaller value of Be_{av} indicates the dominance of fluid flow irreversibilities and thus some available energy is lost leading to less average heating rate. Consequently, case 1 corresponds to a smallest Be_{av} as well as moderate values of Θ_{cup}. In contrast, case 2 corresponds to a lesser fluid flow intensity resulting in smaller values of S_ψ. Therefore, the available energy is larger for case 2 due to smaller fluid friction irreversibilities. As a consequence, Θ_{cup} is larger for case 2 at higher Da. The heat transfer irreversibilities are much larger for case 3 compared to those for cases 1 and 2 and the contribution of S_ψ is less. Thus $Be_{\text{av}} \ge 0.5$ is observed for case 3 and S_{total} is found to be much lesser than that with cases 1 and 2 especially for higher Da. Although S_{total} is less for case 3, but overall thermal mixing temperature is found to be least due to less intense convective transport within the cavity for the entire Da.

The total entropy generation is found to increase with Da for all cases (1–3) with various types of fluids. It is observed that S_{total} in

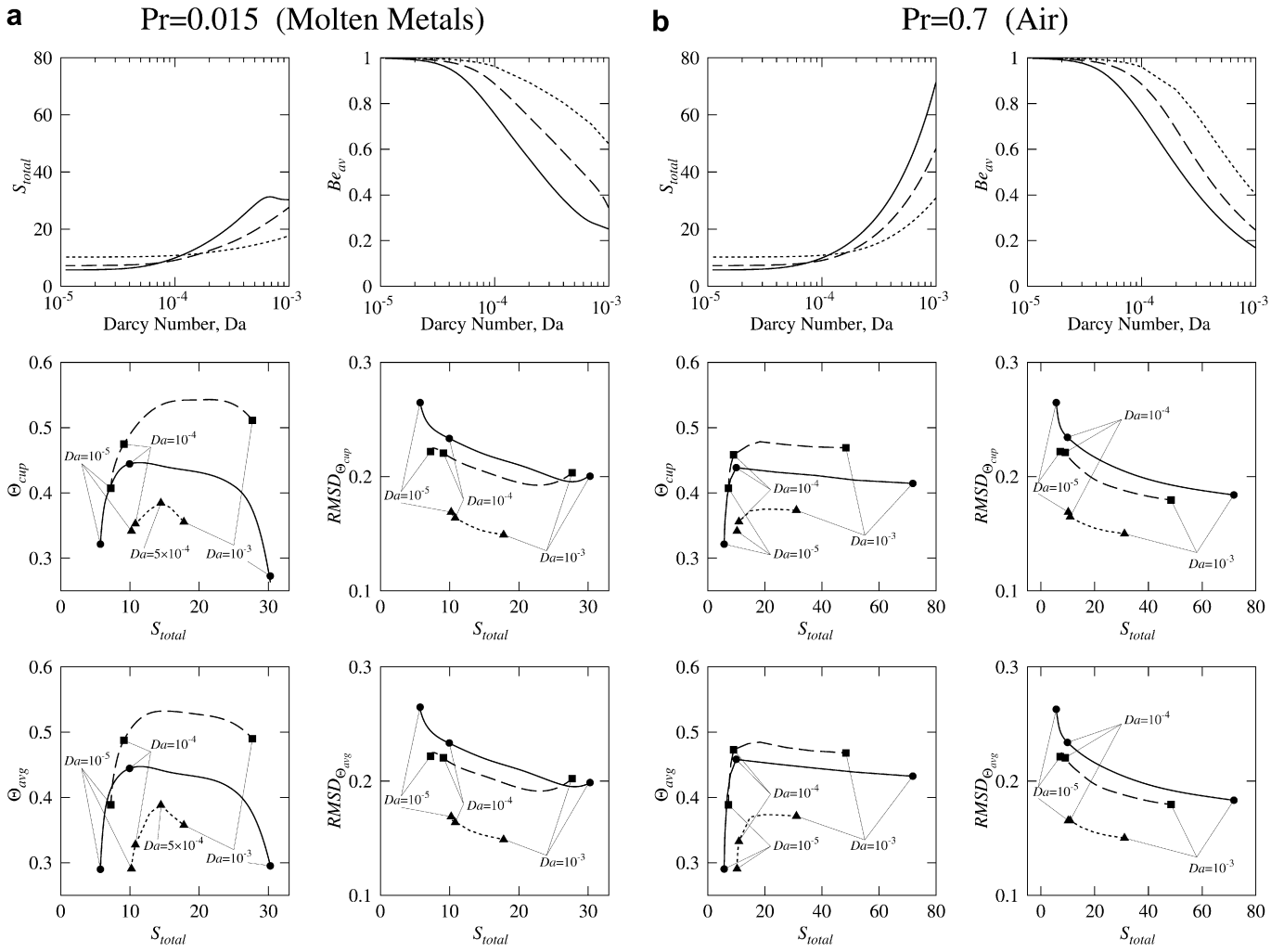

Fig. 12. Variations of the total entropy generation (S_{total}), average Bejan number (Be_{av}) with Darcy number (Da) are shown in the top panels. Distributions of cup-mixing temperature (Θ_{cup}), average temperature (Θ_{avg}) and corresponding root-mean square deviations ($RMSD_{\Theta_{cup}}$ and $RMSD_{\Theta_{avg}}$) as functions of S_{total} are illustrated in the middle and bottom panels. Case 1 (—, ●), Case 2 (– – –, ■) and Case 3 (…, ▲) and $Ra = 10^6$. a and b represent $Pr = 0.015$ and 0.7, respectively.

case 3 is found to be higher during the conduction dominant regime at low Da as the number of hot–cold junctions are more in case 3, resulting in high heat transfer rate and high S_{total}. However, it is interesting to note that, S_{total} in case 3 is observed to be significantly low, compared to that in cases 1 and 2, during the convection dominant regime at higher $Da(=10^{-3})$. The reduction in S_{total} in case 3 is found to be large for high Pr fluids. This may be explained based on the variation of Be_{av}. It may be noted that Be_{av} is maximum and equal to 1 at low Da, indicating the dominance of S_θ. As Da increases, the contribution of S_ψ to S_{total} increases and therefore Be_{av} is observed to be reduced. It may also be noted that, the Be_{av} decreases rapidly in cases 1 and 2 compared to that of case 3. At $Da = 10^{-3}$, the Be_{av} is found to be still >0.5 in case 3 as S_ψ is less dominant for case 3. However, it may be noted that S_ψ dominates the entropy generation at $Da = 10^{-3}$ for higher Pr(0.7,10,1000) fluids, while for $Pr = 0.015$, S_ψ dominates only in cases 1 and 2 and S_θ dominates in case 3, corresponding to $Be_{av} > 0.5$.

Entropy production rates play important role on overall thermal mixing within the fluid of the cavity. It is found that S_{total} is a monotonically increasing function with Da except for case 1 at higher Da for $Pr = 0.015$. Therefore, the thermal mixing or uniformity in temperature for various Da can be correlated. The middle and bottom panels of figures (Figs. 12(a) and (b) and 13(a) and (b)) display mixing effects (Θ_{cup}, Θ_{avg}, $RMSD_{\Theta_{cup}}$, $RMSD_{\Theta_{avg}}$) vs S_{total}. As discussed earlier, higher degree of irreversibility for heat transfer and fluid flow correspond to larger values of S_{total}. It was observed that, a non-monotonic trend of average or cup-mixing temperature vs S_{total} occurs for $Pr = 0.015$ (see Fig. 12(a)). It is found that the values of Θ_{cup} for $Pr = 0.015$ in case 1 attain the maxima and minima. The maxima of Θ_{cup} at higher S_{total} is partly due to enhancement of local thermal mixing due to secondary cells for low Pr fluids. The cup-mixing temperature increases with S_{total} or Da for case 2 and it is observed that there is a slight decrease in Θ_{cup} at higher Da values. It is interesting to note that the variation in S_{total} for $Pr = 0.015$ in case 3 spans only small range and the maxima of Θ_{cup} or Θ_{avg} occurs at an intermediate value of Da as shown in Fig. 12 a.

A common trend on Θ_{cup} or Θ_{avg} vs S_{total} is observed for $Pr = 0.7$, 10 and 1000. It is observed that Θ_{cup} or Θ_{avg} increases with S_{total} till $Da \approx 10^{-4}$ and further, that slightly decreases to reach a constant value at higher Da as well as S_{total}. Smaller values of Θ at higher Da or S_{total} is due to less available energy for heat transport. On the other hand, increasing trend of Θ_{cup} or Θ_{avg} in lower Da regime is partly due to onset of convection leading to enhanced thermal mixing. The convection would not play a significant role beyond a threshold value of Da as larger S_{total} is an indicative of less available heat energy for overall heating. Based on overall entropy

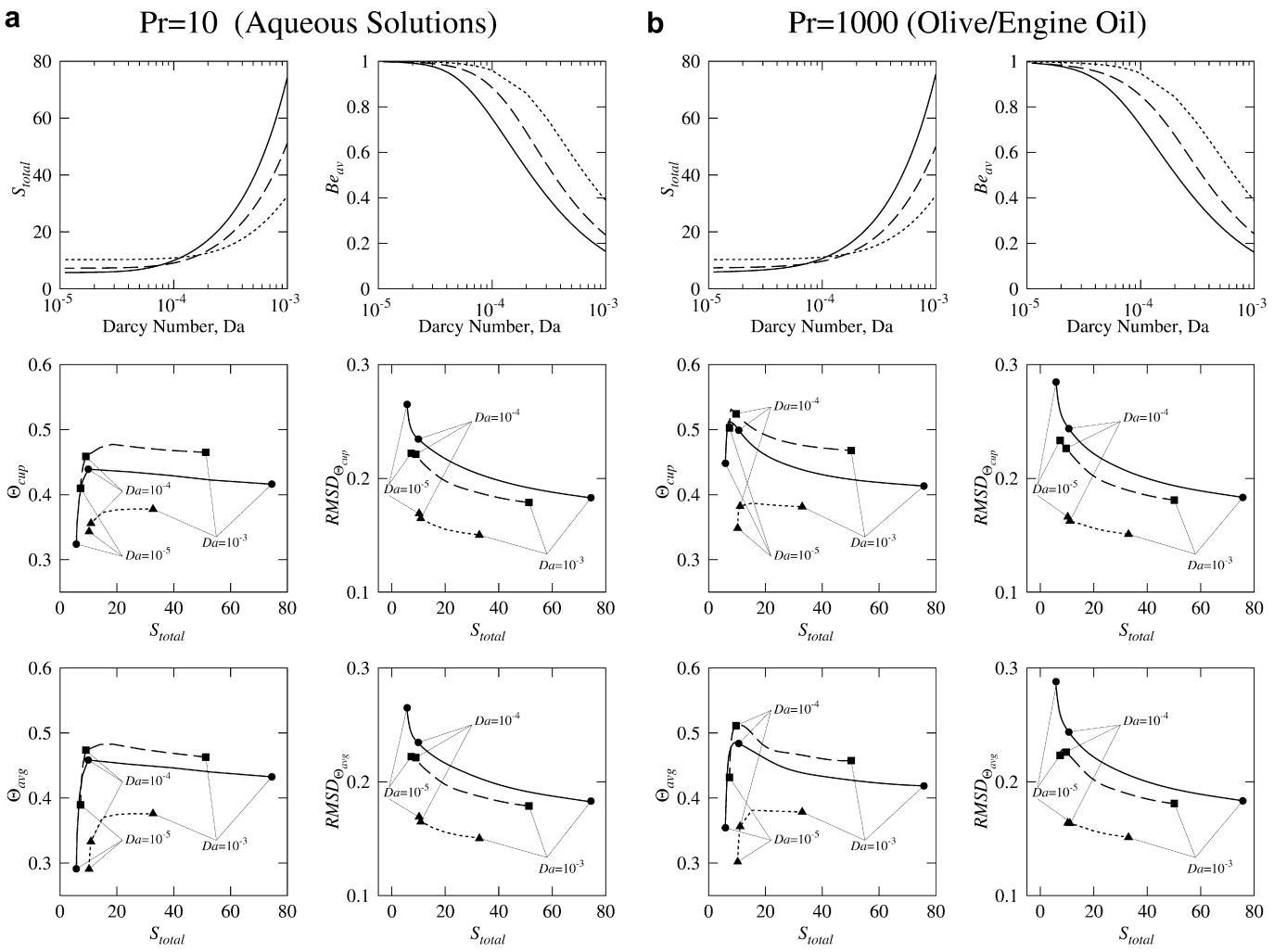

Fig. 13. Variations of the total entropy generation (S_{total}), average Bejan number (Be_{av}) with Darcy number (Da) are shown in the top panels. Distributions of cup-mixing temperature (Θ_{cup}), average temperature (Θ_{avg}) and corresponding root-mean square deviations ($RMSD_{\Theta_{cup}}$ and $RMSD_{\Theta_{avg}}$) as functions of S_{total} are illustrated in the middle and bottom panels. Case 1 (—, ●), Case 2 (– – –, ■) and Case 3 (…, ▲) and $Ra = 10^6$. a and b represent $Pr = 10$ and 1000, respectively.

generation, a critical value of Da may be obtained for optimal thermal processing of various fluids or Pr.

Further, variation of $RMSD_{\Theta_{cup}}$ vs S_{total} indicates that, as the Da increases, the temperature uniformity in the cavity is enhanced due to convection dominance, but on the other hand, the total entropy generation rate also increases. It may be noted that, the temperature uniformity is enhanced (lower value of $RMSD_{\Theta_{cup}}$) for case 2 and that is much enhanced for case 3 at identical parameters. A similar trend is observed for the $RMSD_{\Theta_{avg}}$. It may be noted that the case 3 configuration is characterized by minimum entropy generation in comparison to the cases 1 and 2 for all Pr at high Da. Overall, it may be concluded that employing a case 3 type of configuration for thermal processing of materials would result in moderate thermal mixing, greater degree of temperature uniformity and higher energy efficiency.

The trends of Θ_{cup} or Θ_{avg} and $RMSD_{\Theta_{cup}}$ or $RMSD_{\Theta_{avg}}$ draw a competitive scenario for all fluids. Overall, fluid heating rate is higher at an intermediate value of Da, but the temperature uniformity is achieved at higher Da. On the other hand, higher Da values may not be preferred due to higher S_{total}. This poses an interesting optimization problem to propose an efficient heating strategy with large heating rate (Θ_{cup} or Θ_{avg}), minimal values of $RMSD_{\Theta_{cup}}$ or $RMSD_{\Theta_{avg}}$ as well as minima of S_{total} in presence of optimal distributed heating pattern, which will be a subject of future research.

4. Conclusion

Current work brings new insights on entropy generation during natural convection in porous square cavities heated with differential and distributed heating methodologies. The prime challenge of this work is based on evaluation of entropy generation for heat and fluid flow using finite element based evaluation of derivatives. Total entropy generation in such distributed heating systems has also been analyzed based on spatial entropy maps for various Darcy numbers. Such analysis for distributed heating systems is important to understand entropy generation for efficient thermal processing within porous bed and this has been done for the first time in this work.

A detailed investigations on local and total entropy generation during natural convection in the porous square cavities with differential and distributed heating is presented. Simulations are carried out for wide ranges of permeability of porous medium ($10^{-6} \le Da \le 10^{-3}$) which is saturated with different types of the fluids ($Pr = 0.015, 0.7, 10, 1000$) in the range of $Ra = 10^3$–10^6. A

numerical approach based on the Galerkin finite element method is presented to obtain the local maps of velocity, temperature and entropy generation characteristics.

The effects of permeability of porous medium on entropy generation due to heat transfer and fluid friction irreversibilities are depicted by the local maps of S_θ and S_ψ. Due to low permeability of porous medium at low *Da*, the heat transfer irreversibility is found to dominate the total entropy generation in the cavity. As *Da* increases, the hydraulic resistance of porous medium is reduced and the stronger fluid circulation is observed. Consequently, the irreversibility due to fluid friction is also found to increase and after a critical *Da*, S_ψ dominates the entropy generation (except for $Pr = 0.015$ in case 3). The study on the effect of distributed heating indicates that a significant reduction of S_ψ is observed in case 3 at higher *Da* and *Ra*. Further, it is found that, with the increase in the permeability of porous medium, the case 3 configuration results in lowest S_{total} compared to that in cases 1 and 2. It is also found that, at high *Da*, S_ψ dominates the total entropy generation for higher *Pr* fluids in all cases, whereas the dominance of S_θ is observed for lower *Pr* fluids ($Pr = 0.015$) in case 3 as $Be_{\text{av}} > 0.5$. Comparison of various cases for the total entropy generation indicated that, S_{total} is significantly lower in case 3 with a greater degree of temperature uniformity (smaller $\text{RMSD}_{\Theta_{\text{cup}}}$) across the cavity. The results indicate that a distributed heating methodology based on case 3 type of configuration for thermal processing of materials results in moderate thermal mixing, higher temperature uniformity and high energy efficiency. Finally, current work initiates a study on the optimal heating and processing in a porous bed in order to maximize cup-mixing temperature and temperature uniformity while minimizing total entropy generation at some intermediate Darcy number with an optimal distributed heating policy. What is the critical Darcy number with particular distributed heating policy? This is yet to be resolved and subject to future research.

Acknowledgment

Authors would like to thank anonymous reviewers for critical comments and suggestions which improved the quality of the manuscript.

References

[1] Bejan A. Entropy generation minimization. Boca Raton, FL: CRC; 1982.
[2] Bejan A. Entropy generation minimization: the new thermodynamics of finite-size devices and finite-time processes. J Appl Phys 1996;79:1191–218.
[3] Abbassi H. Entropy generation analysis in a uniformly heated microchannel heat sink. Energy 2007;32:1932–47.
[4] Sciacovelli A, Verda V. Entropy generation analysis in a monolithic-type solid oxide fuel cell (SOFC). Energy 2009;34:850–65.
[5] Satapathy AK. Thermodynamic optimization of a coiled tube heat exchanger under constant wall heat flux condition. Energy 2009;34:1122–6.
[6] Kotcioglu I, Caliskan S, Cansiz A, Baskaya S. Second law analysis and heat transfer in a cross-flow heat exchanger with a new winglet-type vortex generator. Energy; 2010:1–10.
[7] Ordonez JC, Bejan A. Minimum power requirement for environmental control of aircraft. Energy 2003;28:1183–202.
[8] Bidi M, Nobari MRH, Avval MS. A numerical evaluation of combustion in porous media by EGM (entropy generation minimization). Energy 2010;35:3483–500.
[9] Johannessen E, Kjelstrup S. Minimum entropy production rate in plug flow reactors: an optimal control problem solved for SO_2 oxidation. Energy 2004;29:2403–23.
[10] Guo J, Xu M, Cheng L. Thermodynamic analysis of waste heat power generation system. Energy 2010;35:2824–35.
[11] Maveety JG, Razani A. A two-dimensional numerical investigation of the optimal removal time and entropy production rate for a sensible thermal storage system. Energy 1996;21:1265–76.
[12] Nakonieczny K. Entropy generation in a diesel engine turbocharging system. Energy 2002;27:1027–56.
[13] Revellin R, Lips S, Khandekar S, Bonjour J. Local entropy generation for saturated two-phase flow. Energy 2009;34:1113–21.
[14] Nwosu NP. Employing exergy-optimized pin fins in the design of an absorber in a solar air heater. Energy 2010;35:571–5751.
[15] Torres-Reyes E, Navarrete-Gonzalez JJ, Cervantes-de Gortari JG. Thermodynamic optimization as an effective tool to design solar heating systems. Energy 2004;29:2305–15.
[16] Rachedi R, Chikh S. Enhancement of electronic cooling by insertion of foam materials. Heat Mass Transfer 2001;37:371–8.
[17] Keyhani M, Dalton T. Natural convection heat transfer in horizontal rod-bundle enclosures. J Heat Transfer 1996;118:598–605.
[18] Shah A, Brindley J, Griffiths J, Mcintosh A, Pourkashanian M. The ignition of low-exothermicity solids by local heating. Process Saf Environ Protec 2004;82:156–69.
[19] El-Khatib G, Prasad V. Effects of stratification on thermal convection in horizontal porous layers with localized heating from below. J Heat Transfer 1987;109:683–7.
[20] Robillard L, Wang CH, Vasseur P. Multiple steady states in confined porous medium with localized heating from below. Numer Heat Transf Part A: Applic 1988;13:91–110.
[21] Lai FC, Kulacki FA. Experimental study of free and mixed convection in horizontal porous layers locally heated from below. Int J Heat Mass Transfer 1991;34:525–41.
[22] Hsiao SW, Chen CK, Cheng P. A numerical solution for natural convection in a inclined porous cavity with discrete heat source on one wall. Int J Heat Mass Transfer 1994;37:2193–201.
[23] Hadim HA, Bethancourt A. Numerical study of forced convection in a partially porous channel with discrete heat sources. J Elec Packag 1995;117:46–51.
[24] Heindel TJ, Incropera FP, Ramadhyani S. Enhancement of natural convection heat transfer from an array of discrete heat sources. Int J Heat Mass Transfer 1996;39:479–90.
[25] Saeid NH, Pop I. Natural convection from a discrete heater in a square cavity filled with a porous medium. J Porous Media 2005;8:55–63.
[26] Zhao FY, Liu D, Tang GF. Natural convection in a porous enclosure with a partial heating and salting element. Int J Thermal Sci 2008;47:569–83.
[27] Baytas AC. Entropy generation for natural convection in an inclined porous cavity. Int J Heat Mass Transfer 2000;43:2089–99.
[28] Mahmud S, Fraser RA, Pop I. Flow, thermal, energy transfer, and entropy generation characteristics inside wavy enclosures filled with microstructures. J Heat Transfer 2007;129:1564–75.
[29] Zahmatkesh I. On the importance of thermal boundary conditions in heat transfer and entropy generation for natural convection inside a porous enclosure. Int J Thermal Sci 2008;47:339–46.
[30] Varol Y, Oztop HF, Pop I. Entropy generation due to natural convection in non-uniformly heated porous isosceles triangular enclosures at different positions. Int J Heat Mass Transfer 2009;52:1193–205.
[31] Rajesh G, Bhagat RB. Infiltration of liquid metals in porous compacts: modeling of permeabilities during reactive melt infiltration. Trans Porous Media 1999;36:43–68.
[32] Oliveira LS, Haghighi K. Conjugate heat and mass transfer in convective drying of porous media. Numer Heat Transf Part A: Applic 1998;34:105–17.
[33] Jensen TB, Sharma MP, Harris HG, Whitman DL. Numerical investigations of steam and hot-water flooding in fractured porous media. In: SPE 24172, 8th SPE/EOR Sympos, Tulsa, OK, 1992.
[34] Moore RG, Laureshen CJ, Belgrave JDM, Ursenbach MG, Mehta SAR. In situ combustion in Canadian heavy oil reservoirs. Fuel 1995;74:1169–75.
[35] Vafai K, Tien CL. Boundary and inertia effects on flow and heat transfer in porous media. Int J Heat Mass Transfer 1981;24:195–203.
[36] Kaviany M. Laminar flow through a porous channel bounded by isothermal parallel plates. Int J Heat Mass Transfer 1985;28:851–8.
[37] Du ZG, Bilgen E. Natural convection in vertical cavities with internal heat generating porous medium. Wärme-und Stoffübertragung 1992;27:149–55.
[38] Kumar A, Bera P. Natural convection in an anisotropic porous enclosure due to nonuniform heating from the bottom wall. J Heat Transfer 2009;131:1–13.
[39] Reddy JN. An introduction to the finite element method. New York: McGraw-Hill; 1993.
[40] Basak T, Roy S, Balakrishnan AR. Effects of thermal boundary conditions on natural convection flows within a square cavity. Int J Heat Mass Transfer 2009;49:4525–35.
[41] Al -Hadhrami AK, Elliott L, Ingham DB. A new model for viscous dissipation in porous media across a range of permeability values. Trans Porous Media 2003;53:117–22.
[42] Hooman K, Gurgenci H. Effects of viscous dissipation and boundary conditions on forced convection in a channel occupied by a saturated porous medium. Trans Porous Media 2007;68:301–19.
[43] Nield DA, Bejan A. Convection in porous media. 3rd ed. New York: Springer; 2006.
[44] Magyari E, Rees DAS, Keller B. Effect of viscous dissipation on the flow in fluid saturated porous media. In: Vafai K, editor. Handbook of porous media. 2nd ed. New York: Taylor and Francis; 2005.
[45] Gebhart B. Effects of viscous dissipation in natural convection. J Fluid Mech 1962;14:225–32.
[46] Bejan A. On the boundary layer region in a vertical enclosure filled with a porous medium. Lett Heat Mass Trans 1979;6:93–102.

[47] Manole DM, Lage JL. Numerical benchmark results for natural convection in a porous medium cavity. In: heat and mass transfer in porous media. ASME Conf HTD-21; 1992:55–60.
[48] Baytas AC, Pop I. Free convection in a square porous cavity using a thermal nonequilibrium model. Int J Thermal Sci 2002;41:861–70.
[49] Ilis GG, Mobedi M, Sunden B. Effect of aspect ratio on entropy generation in a rectangular cavity with differentially heated vertical walls. Int Commun Heat Mass Transfer 2008;35:696–703.

Nomenclature

Be: Bejan number
Da: Darcy number
g: acceleration due to gravity, m s^{-2}
k: thermal conductivity, W m^{-1} K^{-1}
l′: dimensionless length of hot/cold section
L: side of the square cavity, m
N: total number of nodes
$\overline{Nu}$*:* average Nusselt number
p: pressure, Pa
P: dimensionless pressure
Pr: Prandtl number
R: Residual of weak form
Ra: Rayleigh number
RMSD: root-mean square deviation
S: dimensionless entropy generation
T: temperature of the fluid, K
T_h*:* temperature of discrete heat sources, K
T_c*:* temperature of cold portions of the cavity, K
T_o*:* bulk temperature, K
u: x component of velocity
U: x component of dimensionless velocity
v: y component of velocity
V: *y* component of dimensionless velocity
$\vec{V}$*:* dimensionless velocity
x: distance along *x* coordinate
X: dimensionless distance along *x* coordinate
y: distance along *y* coordinate
Y: dimensionless distance along *y* coordinate

Greek symbols
α*:* thermal diffusivity, m^2 s^{-1}
β*:* volume expansion coefficient, K^{-1}
γ*:* penalty parameter
Γ*:* boundary
θ,Θ*:* dimensionless temperature
μ*:* dynamic viscosity, kg m^{-1} s^{-1}
ν*:* kinematic viscosity, m^2 s^{-1}
ρ*:* density, kg m^{-3}
Φ*:* basis functions
ψ*:* streamfunction

Subscripts
b: bottom wall
c: cold section
h: hot section
j: wall
l: left wall
m: hot or cold section
r: right wall
1,3: cold section
2: hot section
cup: cup-mixing
avg: spatial average